Indian J. Phys. **71A** (4), 471–479 (1997)

IJP A
— an international journal

An X-ray powder profile analysis in cold-worked lead-tin alloys (α-phase)*

Partha Chatterjee and S P Sen Gupta

Department of Materials Science, Indian Association for the Cultivation of Science, Jadavpur, Calcutta-700 032, India

Received 30 May 1997, accepted 11 June 1997

Abstract : A detailed X-ray line profile analysis has been presented initially on three compositions of Pb–Sn alloys in the α-phase prepared by vacuum melting in Pyrex ampoules. Step-scanned X-ray diffraction profiles from cold-worked samples are recorded in a Philips PW 1710 diffractometer interfaced with a computer. Analysis have been done within the framework of Warren-Averbach (WA) method *via* a profile fitting algorithm assuming a Pseudo-Voigt (pV) profile shape function convoluted with an asymmetric function. Since the Pb–Sn alloys tend to decompose after 8 wt % Sn, routine WA analysis leads to fictitious results due to peak overlap. From the shape parameters of true specimen broadened profile the coherent domain sizes, r.m.s microstrain, stacking fault probability, dislocation density are calculated. The values of stacking fault probability are low and do not show appreciable concentration dependence. Cold-working produces very weak structural broadening in Pb–Sn alloys.

Keywords : Pb–Sn alloys, X-ray powder profile analysis, Pseudo-Voigt function

PACS Nos. : 61.10 Nz, 61.72 Hh, 61 72. Nn

1. Introduction

Large amount of work has been done in our laboratory [1] primarily on noble-metal based binary and ternary alloys incorporating X-ray Fourier powder profile analysis of Warren and Averbach [2] in order to characterize the microstructures of plastically deformed state in terms of parameters like coherent domain size, microstrains within those domains, incidence of stacking fault (intrinsic, extrinsic, twin), dislocation density, stacking fault energy *etc*

*Presented at the 8-th Annual General Meeting of Materials Research Society of India (MRSI), held at BARC, Trombay, Bombay, February 10–12, 1997.

We have adopted here a different system— a binary alloy of Pb–Sn in the solid solution range. We have also adopted here recently developed Profile-Fitting approach so as to mathematically carve out the profile tails and parameters pertaining to the profile shape *e.g.* the FWHM, Gaussian/Lorentzian content *etc.* of the X-ray powder profiles.

The Pb–Sn alloys are of commercial importance and are mostly used as "solders." The Pb–Sn alloys were previously studied [3] only in terms of incidence of stacking faults at liquid N_2 temperature. No other work has so far been made to characterize fully the deformed state at room temperature.

Recently, few works have been reported on the microstructure of deformed eutectic alloys [Pb-62 wt% Sn] under tensile stress at high temperature [4]. It has been noted that these alloys show superplastic behaviour which can be attributed to grain boundary sliding [GBS]. This super plastic behaviour is highly sensitive to the presence of grain boundaries and impurities. It has further been noted that for hypoeutectic alloy [Pb-35 wt% Sn] [5], the initial dendritic microstructure transforms into a spheroidized structure as a result of Ostwald ripening on homogenisation. The deformation behaviour is highly sensitive to the grain sizes. Both the eutectic and hypoeutectic alloys fall in the $(\alpha + \beta)$ two phase regime. In view of the above findings the effect of drastic deformation (cold-working) in the α as well as $(\alpha + \beta)$ regime is of considerable importance for investigation.

2. Experimental

Three compositions [Pb-1 wt% Sn; Pb-8 wt% Sn; Pb-12 wt% Sn] of the Pb–Sn alloy system were initially prepared by vacuum melting in Pyrex ampoules. The α-phase is retained by a homogenisation treatment at 200 (±10)°C for 15 days followed by quenching at liquid N_2 temperature.

X-ray diffractograms from cold worked (hand-filed) powders of the alloys prepared at room temperature were taken in a Philips 1710 diffractometer in a step-scan mode with a step size of 0.02° 2θ and counting time of 2 sec per step.

The same alloys were annealed at 180 (±10)°C for 5 hours and the profiles from annealed samples taken under identical conditions were used for peak-shift measurements.

Defect free specially prepared polycrystalline Si powders (with large crystallites) were used as instrument standard.

3. Theoretical approach

Whole Pattern Fitting (Rietveld Method) and/or Profile Fitting is fast becoming an essential tool in profile analysis [6–8]. Rietveld method was originally developed for structure refinement of powder samples using neutron diffraction [6]. Since 1980 it is also used for X-ray diffraction patterns. A review of different profile shape functions have been done by Young and Wiles [7] and it has been found that the Pseudo-Voigt (pV) function is a

reasonable choice with a smaller computation time as compared to the Voigt function which is the best approximation for an X-ray profile. Apart from the usual structure refinement, size-strain analysis has also been incorporated in Rietveld refinement [8]. The size-strain analysis incorporating profile fitting and within the framework of WA method has been done by Enzo *et al* [9,10].

Here we have adopted a Pseudo–Voigt function, defined as :

$$pV(2\theta) = I_0[\eta L(2\theta) + (1-\eta)G(2\theta)] \qquad (1)$$

where $$L(2\theta) = \left[1 + \left\{(2\theta - 2\theta_0)/\omega\right\}^2\right]^{-1}$$

and $$G(2\theta) = \exp\left[-(\ln 2)\left\{(2\theta - 2\theta_0)/\omega\right\}^2\right.$$

η is the Lorentzian content, I_0 is the intensity maxima of $k_{\alpha 1}$ peak $2\theta_0$ the Bragg angle, ω is the half width at half maxima. An asymmetric function :

$A(2\theta) = \exp[-a|2\theta - 2\theta_0/\cot\theta_0]$ is also convoluted with the above pV function to include the effect of axial divergence.

The above function alongwith a linearly varying background is fitted to the experimental data and the parameters related to the profile shape is extracted using the Marquardt non-linear least squares algorithm by the minimisation of the residual :

$$R_w = \left|\Sigma W_i (Y_{iobs} - Y_{ical})^2 / \Sigma W_i Y_{iobs}^2\right|^{1/2}$$

The Fourier transform is calculated according to :

$$F(L) = \left|(1-\eta)(\pi/\ln 2)\exp(-\pi^2\sigma^2 L^2/\ln 2) + \eta\pi\exp(-2\pi\sigma L)\right| \qquad (2)$$

2σ is the FWHM of the $k_{\alpha 1}$ peak expressed in sin θ units The Fourier transform of the 'true sample' is calculated according to Stokes deconvolution as $F(2\theta) = H(2\theta)/G(2\theta)$, where the uppercases F, H, G indicate the Fourier transform of the 'sample', 'experimental' and 'instrumental' profiles respectively.

$F(2\theta)$ is made of two parts :

$F = F_d F_s$ where F_d is the distortion Fourier coefficient and F_s is the size Fourier coefficient.

The size and distortion Fourier coefficients are calculated according to WA method approximating F_d as :

$\exp[-2\pi^2(<\varepsilon_L^2> - <\varepsilon>^2)L^2 n^2 / a_0^2]$, where L is the coherence length, n is the order no. and a_0 is the lattice parameter.

Thus a multiple profile analysis yields the coherent domain size and microstrain within the domains. The column-length distribution function is calculated from the double differentiation of the size Fourier coefficients.

The stacking fault probability α and β are calculated from the peak shift measurements using the relation [11]

$$\delta(\Delta 2\theta) = A(\Delta a/a_0) + H(\alpha' - \alpha'') \tag{3}$$

A and H are constants related by Bragg angle and faulting coefficients. When faulting is taken as the only cause of the observed peak shift the first term of the above equation is neglected. α' is the intrinsic fault probability and α'' is the extrinsic fault probability. β, the twin fault probability is calculated from [11] :

$$4a_0/(4-\sqrt{3})\left(1/D_{\text{eff}}(100) - 1/D_{\text{eff}}(111)\right) = \left[1.5(\alpha' + \alpha'') + \beta\right] \tag{4}$$

where D_{eff} is the coherent domain size.

The dislocation density is calculated using [11] :

$$\rho = (\rho_d \rho_s)^{1/2} \tag{5}$$

where $\rho_s = 3/D_{\text{eff}}^2$, and $\rho_d = k < \varepsilon_L^2 > /b^2$, b is the Burgers vector in the <110> direction and the magnitude is $a_0/\sqrt{2}$, $< \varepsilon_L^2 >$ is the mean square microstrain.

4. Results and Discussion

X-ray diffractograms of cold-worked and annealed samples of three alloy compositions are shown in the Figures 1(a) and 1(b). The alloys tend to decompose after 8% Sn composition. The X-ray pattern of Pb-8-Sn alloy shows 'sidebands' and in Pb-12-Sn alloys, small humps appear due to precipitation effect of Sn, as seen in the diffractogram in Figures 2(a) and 2(b).

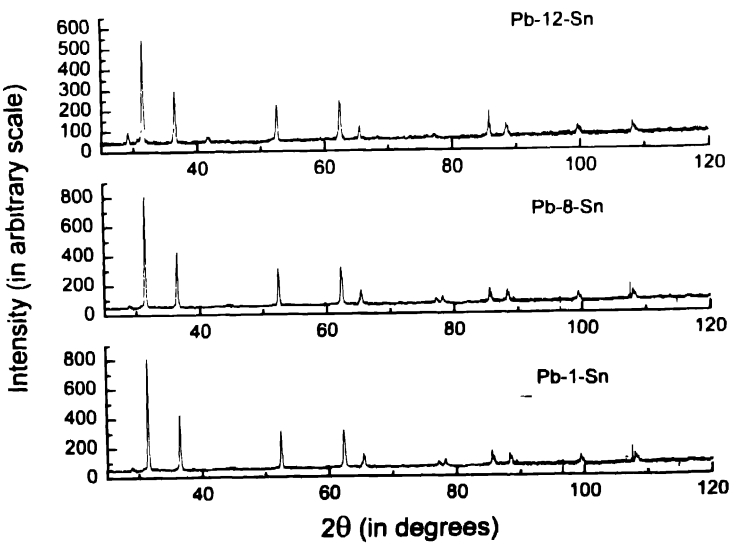

Figure 1(a). X-ray diffraction patterns of cold worked Pb–Sn alloys

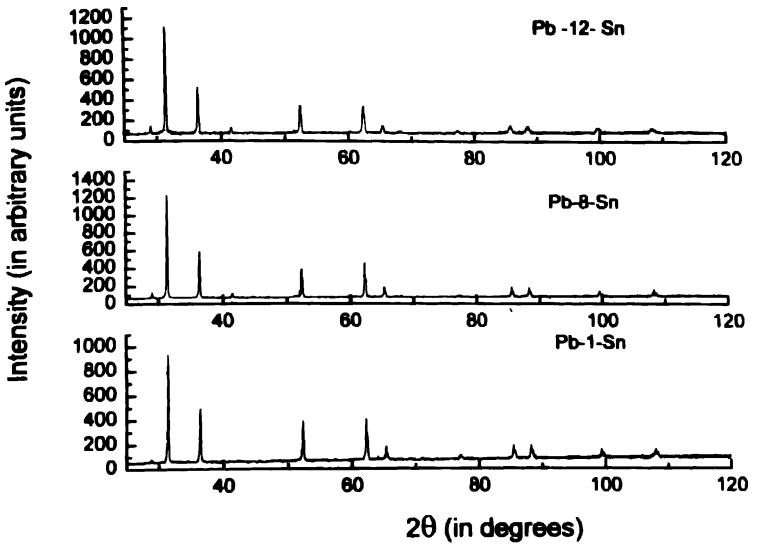

Figure 1(b). X-ray Diffraction patterns of annealed Pb-Sn alloys

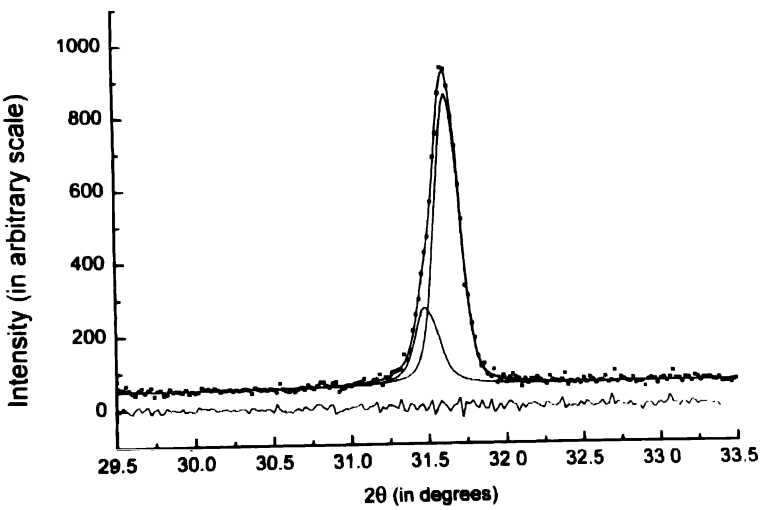

Figure 2(a). Fitted 111 profile of Pb-8-Sn showing the presence of sideband Experimental points alongwith the two fitted peaks are shown Residuals are also shown

Figure 3 shows the plots of lattice parameter values 'a_{hkl}' calculated for different *h k l* planes *versus* extrapolation function cos (θ) cot (θ). The extrapolated lattice parameter [cos (θ) cot (θ) = 0] obtained from a least-squares fit is tabulated in Table 1. It is seen that the values of lattice parameter a_{extrap} of the cold-worked sample decreases with the solute concentration. Similar tendency is noted for the annealed sample which, however, indicates a lattice expansion upon cold-working against the normal lattice contraction effect due to increasing solute concentration.

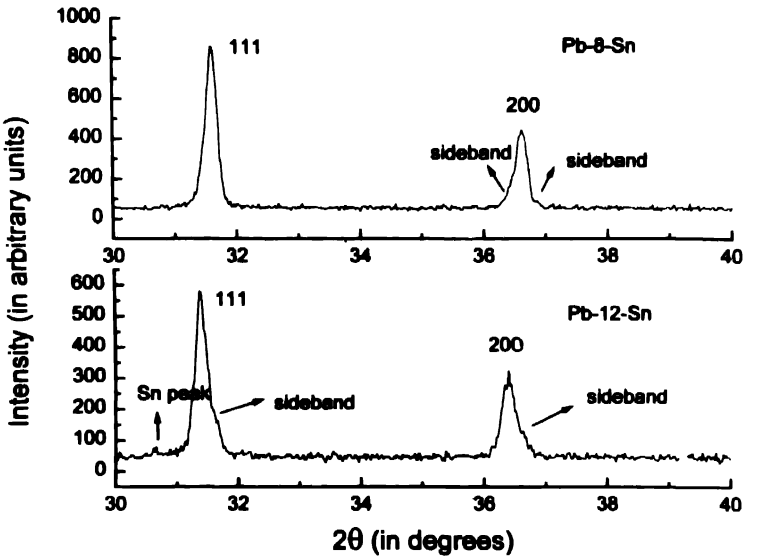

Figure 2(b). X-ray patterns showing decomposition of Pb–Sn alloys

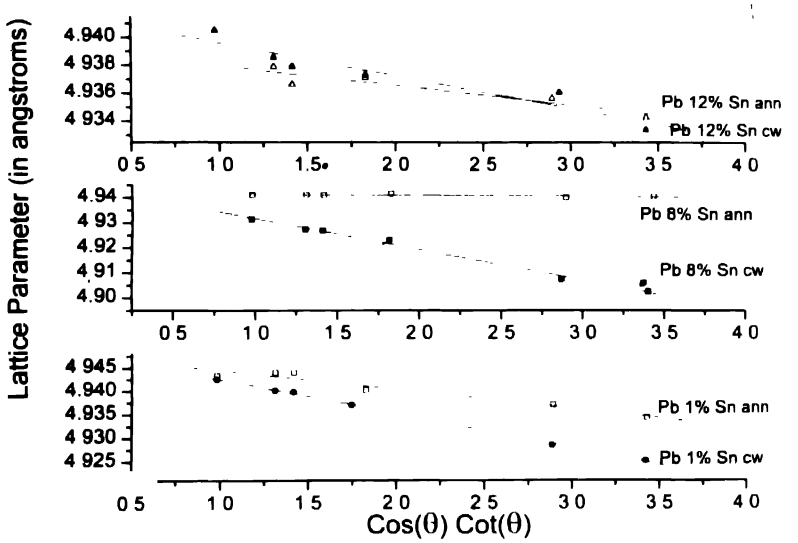

Figure 3. Plot of lattice parameter *vs* extrapolation function.

The mean values of the net deformation stacking fault probability $\alpha > (= \alpha' - \alpha'')$ obtained from the peak shift analysis of the adjacent pairs of reflections assuming (i) faulting effect to be the only cause for observed peak shifts and also (ii) considering the composite effect of the lattice parameter change and faulting (assuming long range residual stresses to be negligible in cold-worked specimen), are shown in Table 2. The values are negligibly small with a little dependence upon solute concentration. The values are less than those obtained by Delhouzee *et al* [3]. This might be due to the fact that we have reported

the values at room temperature which causes a recovery effect as compared to Liq. N_2 temperature data.

Table 1. Values of lattice parameter from cos (θ) cot (θ) plot.

Composition	a_0^{ann} in Å	a^{cw}_{extrap} in A
Pb-1 wt% Sn	4.9485	4.9496
Pb-8 wt% Sn	4.9416	4.9439
Pb-12 wt% Sn	4.9394	4 9419

Table 2. Values of stacking fault probability and lattice parameter

Composition	$\alpha \times 10^{+3}$ (faulting only)	Composite Effect		Lattice parameter a^{cw}_{cal} in Å
		$\alpha \times 10^{+3}$	$\Delta a/a_0 \times 10^{+3}$	
Pb-1 wt% Sn	–3.6	–0.9	–0 5	4 9457
Pb-8 wt% Sn	1 9	–2 8	3	4 9465
Pb-12 wt% Sn	2.3	1.8	5 8	4 9423

The numerically calculated Fourier coefficients F_L of the structurally broadened true '$k_{\alpha 1}$' profile form the basis of the size-strain analysis. A plot of log F_l *versus* l_0^2 ($= h^2 + k^2 + l^2$) produces a set of size dependent Fourier coefficients for different coherence lengths (L) and a column length distribution function can be computed. The column length distribution function is shown in Figure 4. The values of the coherent

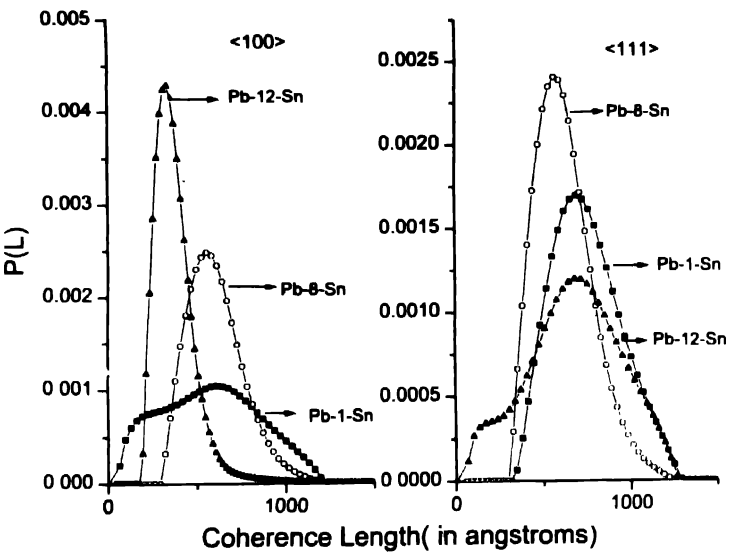

Figure 4. Column length distribution function alog different crystallographic directions.

domain sizes $\langle D_{eff} \rangle$ and the microstrains $\langle \varepsilon_L^2 \rangle$ obtained from the variation of r.m.s. microstrain with L are given in Table 3. Figure 5 shows the variation of microstrains with coherence length (L). It may be seen from Figures 4 and 5 that the values of the coherent

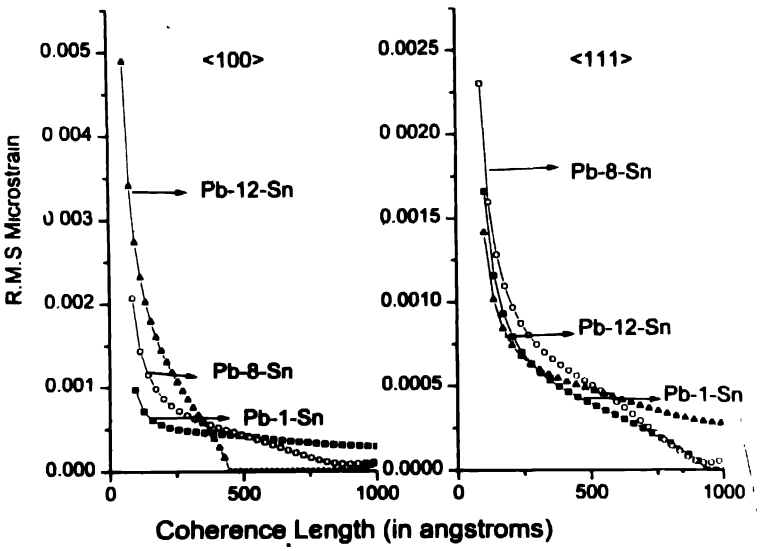

Figure 5. Variation of r.m.s microstrain with coherence length.

domain size decrease with increasing solute concentration with an increase of microstrain within the domains. Pb-8-Sn alloy show a different trend in near-isotropy in the size and strain values. The column length distribution is also identical in the two different crystallographic directions (<111> and <100>).

Table 3. Values of coherent domain size, microstrain, dislocation density and twin fault probability.

Composition	Coherent domain size		R.M.S. microstrain		$\rho \times 10^{-10}$	$\beta \times 10^{+4}$
	<111> in Å	<100> in Å	<111> $\times 10^{+3}$	<100> $\times 10^{+3}$	cm/cm^3	
Pb-1-Sn	735	427	0.43	0.73	2	-
Pb-8-Sn	569	552	0.66	0.58	2.4	-1 4
Pb-12-Sn	520	327	0.57	1.3	5.4	5 4

As peak c.g. could not be found with reliability due to profile overlap, the twin fault probability (β) is calculated from eq. (4) assuming complete absence of extrinsic stacking fault probability (α'') which is a high energy fault. The values of β are also found to be small and the results cannot predict with certainty their presence.

The dislocation density ρ is calculated assuming an absence of dislocation pileups or extensive polygonization [eq. 5]. The values are small and are of the order of 10^{10} cm/cm^3. The values of ρ and β are listed in Table 3.

5. Conclusion

We may conclude the following :

(a) Cold-working in f.c.c Pb–Sn alloys fails to introduce appreciable amount of stacking faults

(b) Crystallite sizes and microstrains are also little influenced by the deformation process.

(c) Decomposition of the alloys after 8% Sn is reflected in the X-ray diffractograms which shows sidebands and indicate inhomogeneous strain. This therefore merits further investigation.

(d) Detailed work is now under progress for the remaining α phase field alongwith the $(\alpha + \beta)$ phase field in order to draw a complete picture of deformation related process and/or the possible influence of the precipitated phase in the matrix.

Acknowledgment

One of the authors (PC) wishes to acknowledge Dr. S K Pradhan for valuable discussions.

References

[1] S K Chattopadhyay, S K Chatterjee and S P Sen Gupta *J. Phys D Appl Phys* **22** 142 (1989), S K Pradhan, A K Maity, M De and S P Sen Gupta *J Appl Phys* **62(4)** 1521 (1987)

[2] B E Warren *X-ray Diffraction*, Addison Wesley, Reading Mass (1969)

[3] L Delehouzee and A Deruyttere *Acta Metall* **15** 727 (1967)

[4] S Yan J C Earthman and F A Mohamed *Phil Mag* **A69** 1017 (1994)

[5] C P Chen and C Y A Tsao *J Mat. Sc* **30** 4019 (1995)

[6] H M Rietveld *J Appl Cryst.* **2** 65 (1967)

[7] R A Young and D B Wiles *J Appl Cryst.* **15** 430 (1982)

[8] L Lutteroti and P Scardi *J Appl. Cryst.* **23** 246 (1990)

[9] S Enzo, A Benedetti and S Polizzi *Z. Kristal.* **170** 275 (1985)

[10] S Enzo, G Fagherazzi, A Benedetti and S Polizzi *J Appl. Cryst* **21** 536 (1988)

[11] S K Chatterjee and S P Sen Gupta *J. Appl. Phys.* **47** 2 411 (1976)